13th International Symposium on Particle Image Velocimetry – ISPIV 2019
Munich, Germany, July 22-24, 2019

Experimental investigation of the fluid-structure interaction between a flexible plate and a periodic gust by means of Robotic Volumetric PIV

Francesco M. A. Mitrotta[1*], Andrea Sciacchitano[1], Jurij Sodja[2], Roeland De Breuker[2], Bas W. van Oudheusden[1]

[1] Delft University of Technology, Faculty of Aerospace Engineering – Section Aerodynamics, Delft, The Netherlands

[2] Delft University of Technology, Faculty of Aerospace Engineering – Section Aerospace Structures and Computational Mechanics, Delft, The Netherlands

[*] f.m.a.mitrotta-1@tudelft.student.nl

Abstract

In the present work Robotic Volumetric PIV is applied in a Fluid-Structure Interaction (FSI) investigation. The case studied involves the dynamic response of a flexible aluminium plate subjected to gust excitation. The experiment is carried out in the Open Jet Facility at Delft University of Technology, which is equipped with a gust generator. Phase-averaged structural displacement of the entire plate together with the volumetric near flow field is measured, with a total measurement volume of approximately 150 litres. Small circular markers are applied to the surface of the plate in order to carry out the structural measurement, which is validated by means of a Scanning Vibrometer. The assessment of the FSI phenomenon is conducted at a wind-tunnel speed of 12 m/s and at a reduced frequency of 0.045. The main aim of this experimental investigation is to demonstrate the capability of Robotic Volumetric PIV to deliver unprecedented quantitative volumetric flow visualization coupled to structural displacement measurement at large scales. The challenges faced to achieve such an objective include the possibility to distinguish between flow particles and structural markers in the acquired images, the validity of the structural displacements measured by the PIV system, the feasibility of the phase-average approach and the consistence of the combined structural and flow information. A visualization of the FSI phenomenon is presented, together with a quantitative analysis of its dynamics.

1 Introduction

The environmental goals set by the European Commission document *Flightpath 2050* (European Commission, 2011) for the European aeronautical industry constitute a drive towards the employment of lightweight aerospace structures. These type of structures are associated with a high degree of flexibility, causing a strong interaction between the air flow and the structural dynamics. This kind of Fluid-Structure Interaction (FSI) is often illustrated by means of the Collar's triangle, that represents the combination of the three different types of force involved in aeroelastic problems: aerodynamic, elastic and inertial. Aeroelastic phenomena are very important when dealing with lightweight structures and they have to be studied both numerically and experimentally in order to ensure the compliance with performance and safety requirements. In the field of wind-tunnel testing, it can be challenging to measure simultaneously the different components of the Collar's triangle. Usually structural characterization is obtained by means of strain gauges, accelerometers, fibre optics and optical displacement measurement, while for aerodynamic assessment pressure sensors and force balances are the main tools (see e.g. Ballmann et al., 2008; Silva et al., 2012). Quantitative flow visualization is rarely used, preventing a complete aerodynamic characterization of aeroelastic phenomena to be achieved.

In the last decades, Particle Image Velocimetry (PIV) has emerged as the main technique for quantitative flow visualization in a wind-tunnel environment. However, its combined employment with simultaneous structural measurements is reported in only a few works in literature. Some of these deal with the FSI

related to Micro-Air-Vehicles (MAVs) and make use of planar PIV coupled to Digital Image Correlation (DIC) to perform full field deformation measurements of membrane wings. For instance, Timpe et al. (2013) assess the passive flow control mechanism of a free trailing-edge scalloped membrane wing by means of synchronized, time-resolved PIV and DIC. A similar PIV-DIC coupling is used by Bleischwitz et al. (2017) to investigate a flexible membrane wing in free-flight and ground-effect conditions. A combination of stereoscopic PIV and DIC is presented in Marimon Giovannetti et al. (2017), where the deformation of a rectangular wing and the displacement of the induced tip vortex are investigated under steady inflow conditions at different wind-tunnel speeds. As far as volumetric flow measurement is concerned, an example is given in Kalmbach and Breuer (2013), where the authors propose an experimental benchmark for a generic FSI test case. This test case involves a rigid cylinder with a flexible tail, where the vortex shedding induces dynamic deformation of the tail. Planar PIV and volumetric V3V measurements of the flow are separately coupled with deformation measurement obtained by means of a multiple-point laser triangulation sensor. Finally, a combination of PIV-based pressure and deformation measurement can be found in Zhang et al. (2019). In this work, planar PIV is coupled to DIC in order to assess the hydrodynamic loading and structural response of a steady flow impinging on a cantilevered flexible plate.

Despite the combination of quantitative flow visualization and structural measurements, the mentioned works do not attempt to calculate the surface pressures associated with the PIV flow field in order to establish a link with the structural displacements. Only Zhang et al. (2019) perform pressure reconstruction from the measured flow field; however their study is limited to a steady 2D flow. A large variety of aeroelastic phenomena involves the presence of 3D unsteady flows and large scale structures, making the experimental assessment of the components of Collar's triangle dependent on the availability of volumetric flow measurement in unsteady flows over large volumes.

In the field of large-scale aerodynamic measurements, the introduction of Robotic Volumetric PIV (Jux et al., 2018) has revealed a large potential for volumetric measurements in domains of several cubic meters. The technique comprises the manipulation of a Coaxial Volumetric Velocimetry (CVV) probe (Schneiders et al., 2018) by means of a robotic arm, in combination with Helium-Filled Soap Bubbles (HFSB, Scarano et al., 2015) as flow tracers and the Lagrangian Particle Tracking (LPT) algorithm Shake-the-Box (STB, Schanz et al., 2016) for image processing. Jux et al. (2018) demonstrate the operation of Robotic Volumetric PIV by measuring the time-averaged velocity field around a full-scale cyclist mannequin. The final measurement volume is approximately 2000 litres large, resulting from the acquisition of 450 independent views. Robotic Volumetric PIV is applied to an unsteady flow in the study of Martínez Gallar et al. (2018), where the near wake topology of a flapping-wing MAV is studied and the flow field is obtained by means of a phase-locked averaging procedure. A measurement volume of 60 litres is achieved in this latter case, making use of 4 independent views.

The present work demonstrates the use of Robotic Volumetric PIV for the simultaneous measurement of structural displacements and volumetric unsteady flow field over a large scale model. The investigated case consists in a flexible aluminium plate excited by a periodic gust. The structural displacements measured by the Robotic Volumetric PIV system are validated with simultaneous measurements performed with a Scanning Vibrometer (SV). The phase-averaged structural displacements and flow field are combined together in order to present a full visualization of the FSI phenomenon.

2 Experimental Setup

2.1 Wind-tunnel

The experiment is conducted in the Open Jet Facility (OJF) at Delft University of Technology. This is a closed-loop, open test section wind-tunnel with an octagonal outlet section of 2.85×2.85 m^2 and a maximum achievable free-stream velocity of 35 m/s (TU Delft, 2019). The contraction ratio is $3:1$ and the turbulence intensity is reported to be lower than 0.5% at 1 m from the tunnel nozzle (Lignarolo, 2016).

2.2 Gust Generator

The gust generator is a device developed by the Aerospace Structures and Computational Mechanics Section of the Aerospace Faculty of Delft University of Technology for the generation of gusts in the test section of the OJF. Its design and characterization is reported in Lancelot et al. (2017b) and Lancelot et al. (2017a). Here the main features are mentioned for completeness sake.

The gust generator is installed in front of the outlet section of the wind-tunnel and it is composed of an aluminium frame, two active wings called gust vanes and a system for actuation and control. The function of the aluminium frame is to support the gust vanes and the actuators, so for this reason it is fixed to the ground. The gust vanes are two wings mounted vertically in the frame and they are made from foam which is supported by an aluminium spar. Their span is 2.88 m in order to cover the full height of the outlet section. The airfoil of the gust vanes is a NACA 0014 and the chord has a length of 0.3 m. The spacing between the two gust vanes is 0.7 m. When the gust generator is operated, the gust vanes are deflected in order to generate a transverse velocity component with respect to the free-stream. The actuation and control system is needed to impose a deterministic motion to the gust vanes in order to obtain the desired gust profile in the flow. The system is controlled by means of a gust generator interface implemented in the *National Instrument* LABVIEW environment.

2.3 Test Object

The test object is a thin rectangular plate made of 7075 aluminium alloy. This type of aluminium has a density of 2810 kg/m^3 and a a Young modulus of 71.7 GPa. The span of the plate is 1217.5 mm, while the chord and the thickness are 170.0 mm and 2.5 mm respectively. Circular markers with a diameter of 1.5 ± 0.2 mm[1] are painted on the surface of the plate. The markers are applied on both sides of the plate in order to have a reference for the SV when simultaneous measurements with the Robotic Volumetric PIV system are performed. The arrangement of the markers consists in 34 rows of 5 markers with uniform spacing of 35 mm. In the wind-tunnel, the aluminium plate is clamped vertically on a support table by two L-shaped flanges, to simulate a clamped boundary condition. All the free edges of the plate are milled with a radius of 1 mm. An illustration of the clamp mechanism and of the markers' arrangement is given in Figure 1. The combination of a high aspect ratio (7.16) with a very small thickness relative to the other dimensions guarantees a large flexibility of the plate. The first eigenfrequency of the presented configuration is approximately 1.6 Hz, while the expected maximum tip displacement for the different measurement cases is estimated to be 11 cm (9% of the span)[2].

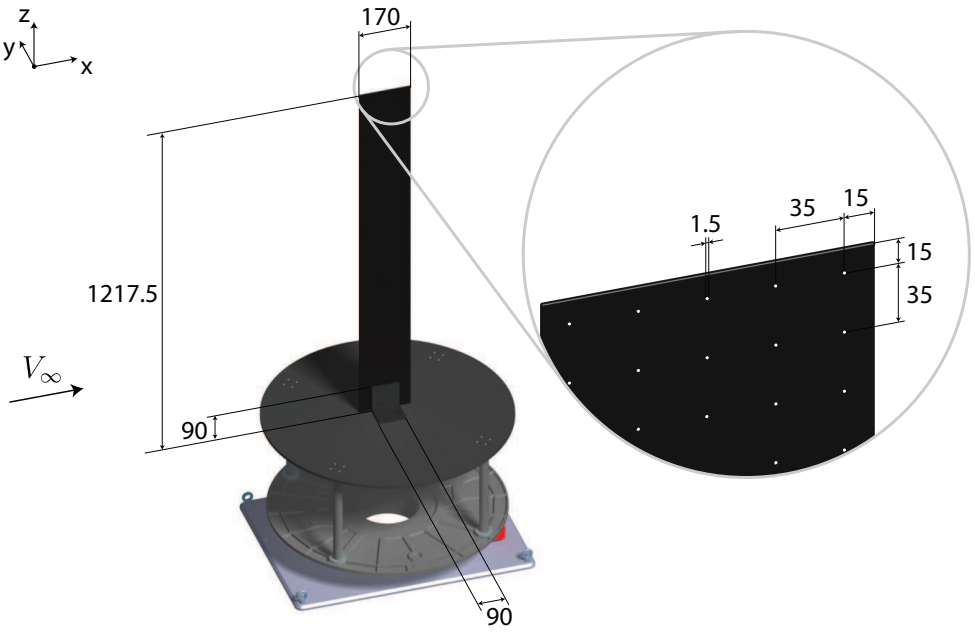

Figure 1: Model of the aluminium plate clamped to the support table and zoom-in of the plate's tip with markers; all dimensions in millimetres

[1]The markers are obtained by applying a laser cut mask on the plate and spraying some paint. The mask manufacturer claims that the lines cut by the laser can be at most 0.2 mm wide.

[2]The eigenfrequency and tip displacement estimations are based on numerical simulations carried out in the software MSC NASTRAN.

2.4 Measurement Systems

Two measurement devices are used in the present experimental investigation: a Robotic Volumetric PIV system and a Scanning Vibrometer (SV). The former is constituted by the *LaVision* CVV probe *MiniShaker Aero* installed on a *Universal Robot UR5* collaborative robotic arm. The light source is provided by a *Quantronix Darwin-Duo* Nd-YLF laser, having a light wavelength $\lambda = 527$ nm and a pulse energy of 2×25 mJ at 1 kHz. The *MiniShaker Aero* is equipped with four CMOS cameras having lenses with 4 mm focal length and sensor with a pixel pitch equal to 4.8 μm and a bit depth equal to 10. Furthermore, in order to obtain a maximum acquisition frequency of 821 Hz, the active sensor is reduced to 640×475 pixels. The seeding of HFSB in the flow is provided by an in-house developed rake of ten wings with 20 nozzles each, resulting in an overall cross-section of 0.5×1 m^2. This seeding rake is placed in the settling chamber of the wind-tunnel in order to increase the particle concentration in the test section and reduce the turbulence intensity generated by the rake itself. A *LaVision* digital Fluid Supply Unit (FSU) is used to control the seeding rake distributor. The Robotic Volumetric PIV system is completed by an acquisition computer providing the *LaVision* software DaVis 10.0.5 to control both the PIV acquisition and the robotic manipulation. The average number of particles-per-pixel (ppp) observed in the acquired images is 0.0018 and the seeding concentration obtained considering the average acquisition volume is approximately 0.0328 bubbles/cm^3. The total measured volume corresponds approximately to 150 litres.

The SV used in this experiment is the *Polytec PSV-500 Scanning Vibrometer*[3] (Polytec, 2018). This is a laser Doppler vibrometer used for full-field non-contact vibration measurements. It can determine the vibration velocity at a selected point by means of the Doppler effect, sensing the frequency shift of back scattered light from a moving surface. Displacement and acceleration can also be obtained by means of integration and differentiation, respectively. The resolution of the measured velocity is at worst 14 μm/s. The SV is placed on the opposite side of the model with respect to the Robotic Volumetric PIV system. In this way the vibrometer laser can point at the plate surface that is not illuminated by the PIV laser, so that light source contamination is avoided.

Finally, the two measurement systems are synchronized between themselves and with the gust generator. The synchronization is obtained with a trigger signal sent from the gust generator controller to both the Robotic Volumetric PIV and the SV systems. Additionally, electric signals from the gust generator and the two measurement systems are acquired by means of a *National Instrument* acquisition station controlled by a purpose-developed interface in the LabVIEW environment. These signals include the measured angle of the gust vanes and the acquisition signals from the Robotic Volumetric PIV and the SV systems. Such operation is needed for the phase reconstruction of the investigated periodic phenomenon.

A complete overview of the experimental setup is given in Figure 2. The reference frame used for the PIV measurements is also shown in the figure, which has its origin at the floor centre-point of the wind-tunnel outlet section.

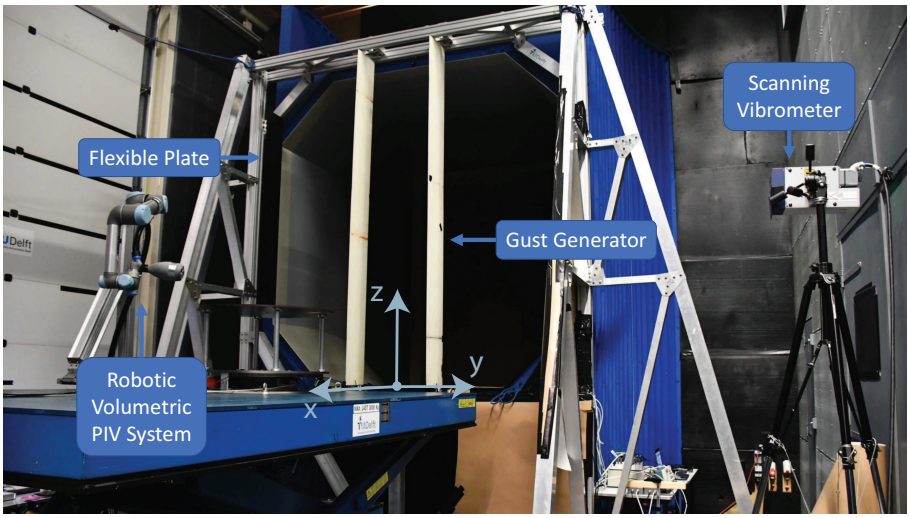

Figure 2: Illustration of the experimental setup

[3]The system used is a *PSV-500-B* with a *PSV-I-550 Scanning Head Xtra*.

2.5 Measurement Procedure

The investigated FSI phenomenon consists in the response of the aluminium plate to a continuous gust excitation. Therefore, the gust vanes are actuated in a sinusoidal fashion in order to generate a periodic sine gust. Three different sets of measurement are carried out during the experiment. The first set consists of simultaneous Robotic Volumetric PIV and SV acquisition, without HFSB seeding. This offers a clean validation case for the structural measurements of the Robotic Volumetric PIV system. During the second set of measurements, the HSFB generator is switched on. In this way, the capability of the Robotic Volumetric PIV system to deliver valid structural measurement in the presence of flow tracers can be assessed. Finally, the third set of measurements involves the use of the Robotic Volumetric PIV system for the measurement of the FSI phenomenon over the entire span of the plate. The physical and acquisition parameters of each set of measurements are shown in Table 1. The PIV acquisition frequency is reduced when no HFSB are used in order to store a smaller amount of data. This is justified by the fact that the plate is supposed to respond with the same frequency as that of the gust (0.9 Hz), which is very small with respect to the acquisition frequency and it entails a lower frequency requirement for the tracking of structural markers with STB. Furthermore, a smaller gust amplitude is employed when the Robotic Volumetric PIV system is used simultaneously with the SV. This is done with the aim of providing an experimental condition where the SV can be regarded as ground truth, since for large displacements of the plate the point measured by the SV experiences a substantial motion over the plate surface and it cannot be considered fixed. For the real investigation of the FSI phenomenon a large gust amplitude is desired for a clear observation of the dynamic behaviour of both flow and structure.

Each session of data acquisition is performed in loops of data recording separated by a certain amount of saving time. For each session, the gust generator is started and the measurement systems are kept on hold until the transient has died out. The PIV and SV acquisition of the first loop is started by means of a trigger signal sent by the gust generator controller. About 5 seconds before that, the recording of the electric signals is started manually. Once the first loop has been acquired, the gust generator stops and the measurement systems save the acquired data. From the second loop onwards the described operations are automatized and repeated for the desired number of loops.

Table 1: Physical and acquisition parameters of the studied measurement cases

	PIV - SV - no HFSB	PIV - SV - HFSB	PIV - HFSB
Physical parameters			
Wind-tunnel speed [m/s]	11	11	12
Gust reduced frequency	0.044	0.044	0.045
Gust vanes deflection [deg]	5	5	10
Acquisition parameters			
PIV acquisition frequency [Hz]	200	821	821
SV acquisition frequency [Hz]	1000	1000	
# gust cycles per acquisition	20	20	20
PIV images per acquisition	4400	18076	16433
# PIV volumes	3	3	14
# acquisition loops per PIV volume	1	1	8
SV samples per acquisition	2200	2200	
# SV points	9	6	

3 Methodology

3.1 Flow and Structure Image Separation

The PIV images acquired with the active HFSB generator contain both flow and structure tracers. The first challenge in the measurement of the FSI phenomenon is to obtain separate sets of images for flow and structure. This problem is tackled by making the hypothesis that, on average, structural markers move much slower with respect to flow particles. With this assumption, it is possible to use image pre-processing operations based on time-series to separate flow from structure. A time minimum filter is employed to obtain an image set with only structural markers. This filter retains the minimum intensity for each pixel over a certain number of consecutive images. Since structural markers occupy the same pixels for a larger number of images with respect to flow tracers, the latter can be eliminated by taking the minimum over a small enough number of images. A size of 3 images is selected as kernel of the filter. For the elimination of structural markers the temporal high pass filter proposed by Sciacchitano and Scarano (2014) is used. This filter is based on the decomposition of the pixel intensity signal in the frequency domain, where the low-frequencies, associated with reflections from steady and slow-moving surfaces, are filtered out. Once separate flow and structure images are obtained, a further set of image pre-processing operations is applied. These operations include subtraction of sliding minimum and local normalization of the pixel intensity with the aim of achieving nicely shaped particle images with homogeneous intensities and zero background (LaVision, 2018). An example of the pre-processed flow and structure images is shown in Figure 3.

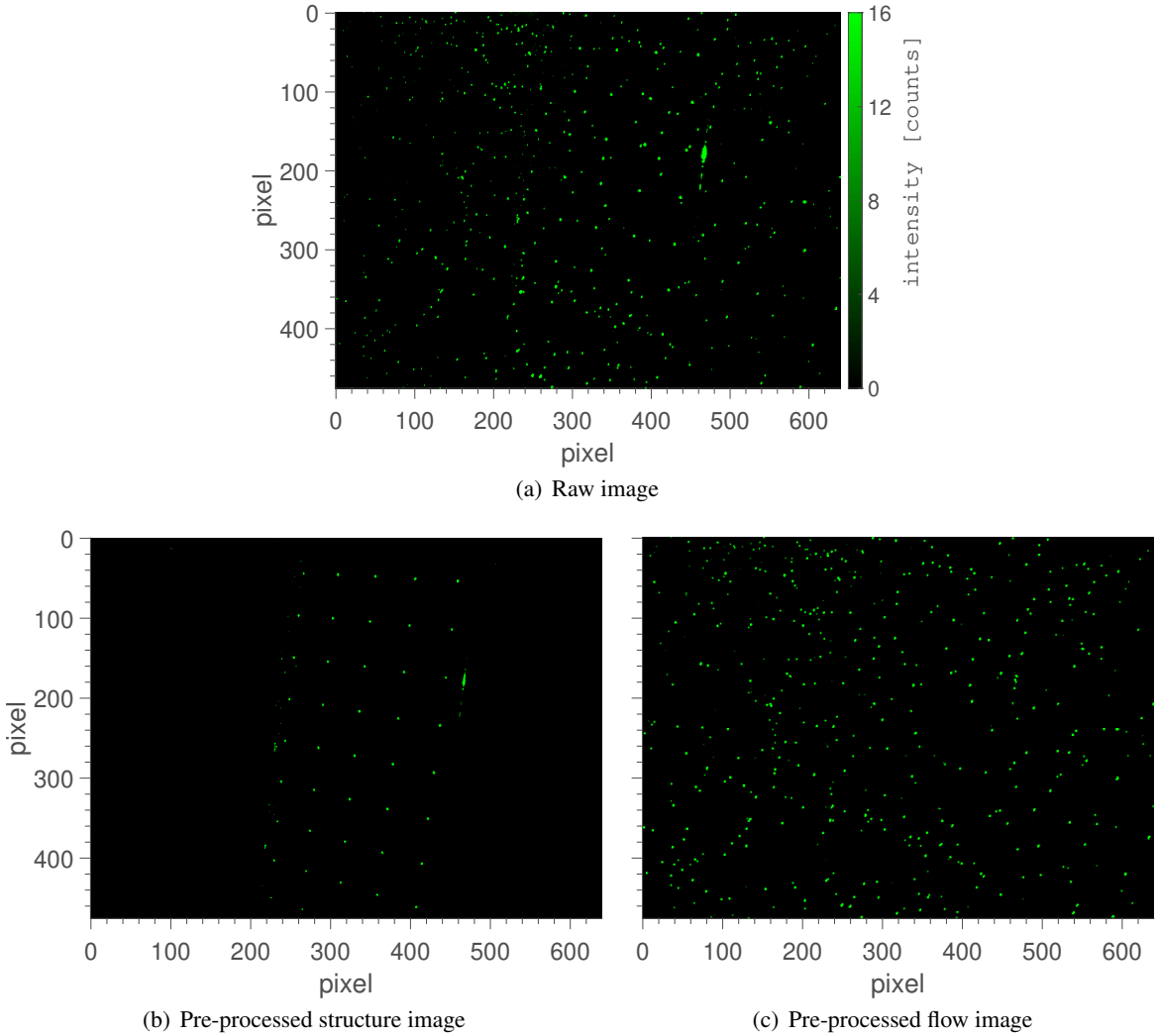

(a) Raw image

(b) Pre-processed structure image

(c) Pre-processed flow image

Figure 3: Raw image and pre-processed images with separated structural markers and flow tracers

3.2 Structure Processing

The assessment of the plate's structural response relies on the possibility to measure the markers' displacement by means of the LPT algorithm STB. For the application of STB, the calculation of a volume self-calibration (Wieneke, 2008) and an optical transfer function (OTF, Schanz et al., 2012) is recommended. To perform these operations, a specific dataset including marker images from different acquisitions is created. Since markers look similar to flow tracers in the pre-processed images, a volume self-calibration and an OTF based on flow images may be used for structure processing. However, the previously described strategy is employed because it has been observed to provide significantly better results. The application of the STB algorithm to the structure images is performed via the use of 8 iterations for both outer and inner loop and by a 0.05 *vox* shaking. This is done to compensate the significant instantaneous particle positional error of the CVV probe along the imaging direction (in the order of 1 mm, Schneiders et al., 2018). The consequent high computational cost is affordable given that the number of tracks in a structure dataset is several order of magnitude lower than the one in a flow dataset.

The STB processing results in several tracks for each marker. In order to describe the instantaneous displacement over the entire acquisition time, an algorithm is developed to join the tracks associated with the same marker. For the calculation of the phase-averaged displacement of the markers, the following strategy is employed. Assuming a periodic behaviour for the FSI phenomenon, a least square regression of a sine wave is performed on the recorded signal of the gust vanes' angle. The periods and the phase shifts of the two sine waves obtained from the regression are averaged in order to obtain a reference periodic signal with period T_{ref}. T_{ref} is used to define the period of the FSI phenomenon. Each period is divided into a certain number of phases. The starting point of the first cycle is defined by the closest time instant preceding the start of the acquisition and corresponding to a phase angle multiple of 2π. The marker displacements are linearly interpolated to the time instants corresponding to the desired phases. Displacements belonging to the same phase are then averaged together.

3.3 Flow Processing

For the processing of the flow images, a volume self-calibration and an OTF are also needed. The same procedure employed for structure images is used here for flow images. The STB algorithm is applied in this case using 4 iterations for both outer and inner loop and a 0.1 *vox* shaking. Once a Lagrangian description of the flow is obtained, a phase-average approach is employed to convert the information into an Eulerian description on a structured grid. The technique used to determine the phases and the corresponding time instants within the acquisition time is analogous to the one used for the structure. A spline interpolation is employed to interpolate particles' position and velocity to the various phases of the different cycles. For each phase an ensemble average is carried out in an analogous way as illustrated by Jux et al. (2018). Inspired by the approach proposed by Agüera et al. (2016), here a linear regression for the velocity components is used for the spatial averaging inside each cubic cell of the structured grid.

The Eulerian description of the flow and the Lagrangian description of the structure are finally mapped to a common global reference system, in order to allow a visualization of the FSI phenomenon.

4 Results

4.1 Validation of Structural Displacement

The validation of the instantaneous displacements measured by the Robotic Volumetric PIV system is initially carried out using the measurement set involving simultaneous PIV and SV acquisition without HFSB. Some markers along the span of the plate are selected and measured one at a time. Figure 4(a) shows the comparison between Robotic Volumetric PIV and SV measurements for the centre-chord marker belonging to the row located at 55% of the plate span. The displacement shown in the figure is the one measured from the first detected position of the marker. The bias error $\varepsilon_{b,\Delta y}$, calculated from 20 gust cycles, results in $\varepsilon_{b,\Delta y} \approx -0.258$ mm, while the random error $\varepsilon_{r,\Delta y}$ is approximately 0.718 mm. Since inertia forces depend on accelerations, it is important to evaluate the related measurement performance of the Robotic Volumetric PIV system. Accelerations are calculated from the displacement data of both systems employing a sliding least square regression of a third order polynomial, using a kernel of 1/4 of the known gust period. The polynomial is derived twice in time and the acceleration is evaluated at the desired time instant. The comparison between Robotic Volumetric PIV and SV results is shown in Figure 4(b), together with their difference. In this case the bias and random errors are respectively $\varepsilon_{b,a_y} \approx -0.001$ mm/s^2 and $\varepsilon_{r,a_y} \approx 0.270$ mm/s^2.

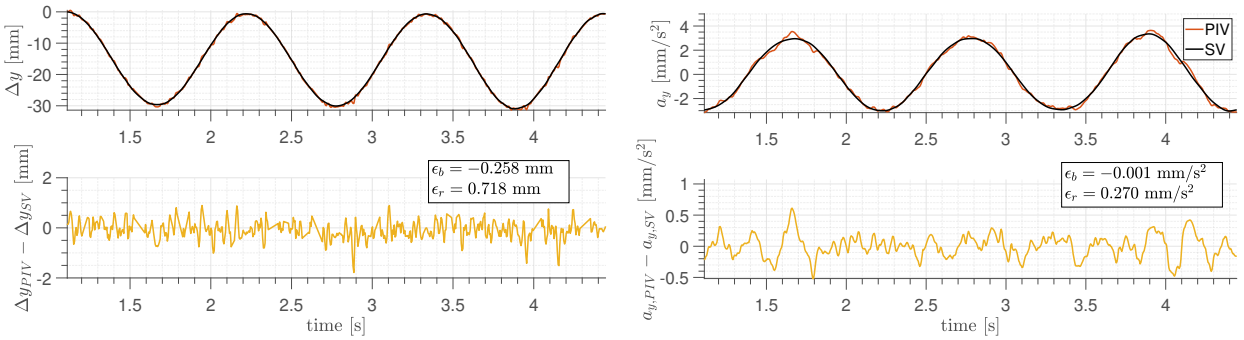

(a) Structural displacement

(b) Structural acceleration

Figure 4: Comparison between instantaneous PIV and SV measurements

4.2 Phase-average Approach

Given the small seeding concentration obtained and the periodic character of the investigated phenomenon, a phase-average approach is employed to average the instantaneous results of both flow and structure over different cycles. In order to quantify the extent of the validity of the phase-average approach, the scatter in the structural displacements from one cycle to the other is assessed here. Three different kinds of measurement are compared: SV without HFSB, PIV without HFSB and PIV with HFSB. The same marker previously considered is used here to obtain the phase-averaged displacements over 20 cycles. The results are shown in Figure 5. The scatter among the different cycles is indicated by means of error bars that have a length of twice the standard deviation calculated for each phase. The average standard deviation over the entire averaged cycle is approximately 0.366 mm, 0.784 mm and 0.717 mm for SV without HFSB, PIV without HFSB and PIV with HFSB, respectively. If the random error related to the SV system is considered negligible, then the first value can be mainly attributed to the scatter among the gusts generated in the different cycles, while the last two values include both the gusts scatter and the PIV measurement error with comparable importance. Furthermore, considering the same order of magnitude for the average standard deviation of PIV - no HFSB and PIV - HFSB configurations, it can be inferred that the introduction of HFSB does not compromise the structural measurement performed with the Robotic Volumetric PIV system.

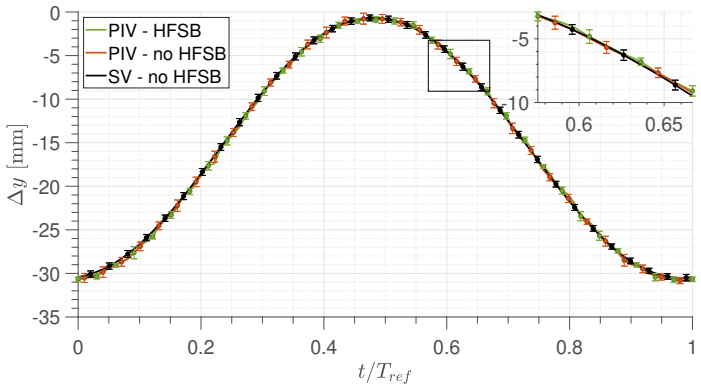

Figure 5: Phase-averaged structural displacements

4.3 FSI Visualization

The combination of the description of flow and structure permits to visualize the full FSI phenomenon, as it is done in Figure 6. Two independent views of the PIV - HFSB measurement set including the marker analysed beforehand are used to produce the results shown, thus representing only a part of the plate and of the total measurement volume. Three different phases of the gust cycle are presented, namely $t/T_{ref} = 0.5$,

$t/T_{ref} = 0.75$ and $t/T_{ref} = 1$. According to the results of Figure 5, these phases correspond respectively to the plate being at the farthest point, at an intermediate point and at the closest point with respect to the CVV probe. A 3D view of the phase corresponding to $t/T_{ref} = 0.5$ is shown in Figure 6(a). The flow is inspected by means of a slice at $z = 1.147$ m (54.4% of the plate span) coloured with the streamwise component of the flow velocity, u, and seeded with 2D streamlines. Additionally, a $u = 10.5$ m/s iso-surface (corresponding to a nominal $u/u_\infty = 0.875$) is plotted in order to visualize the deceleration of the flow along the span of the plate with respect to the free-stream. This lower u component close to the leading edge of the plate suggests that, for the considered phase, the measured side of the plate acts as a pressure side. This can be further assessed in Figure 6(b), where the same slice is shown from the top in a 2D view. Here the contour of the decelerated flow region can be observed again, together with the 2D vector field. The flow deceleration is caused by a certain angle of attack of the flow seen by the plate, which is in turn the effect of the combination of the gust field and the velocity of the plate itself. The contribution of the velocity of the plate to the effective angle of attack will be analysed later. The results of the other two phases of the cycle are presented in Figure 6(c) and 6(d). In the former, corresponding to $t/T_{ref} = 0.75$, both the plate and the measured flow field have moved along the y axis and the flow appears to be undisturbed with respect to the free-stream. The last phase shows instead a region of accelerated flow, indicating that the measured side of the plate is acting as a suction side. Besides, both the plate and the measured flow field have moved further along the y axis.

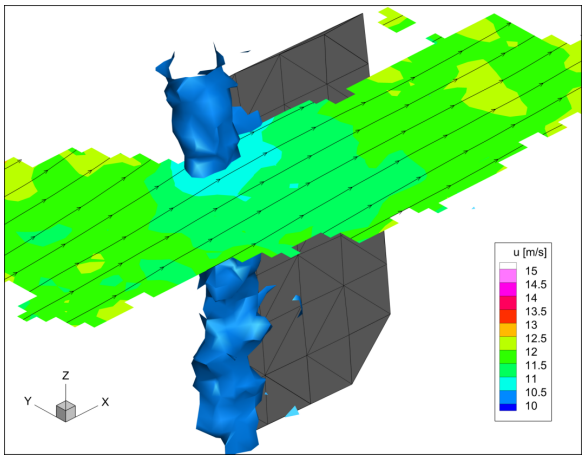

(a) 3D view at $t/T_{ref} = 0.5$. Iso-surface of $u = 10.5$ m/s

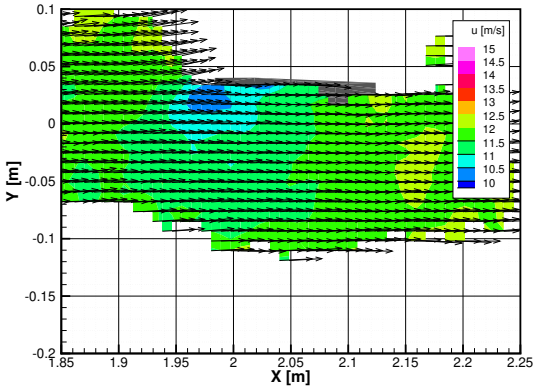

(b) 2D top view at $t/T_{ref} = 0.5$

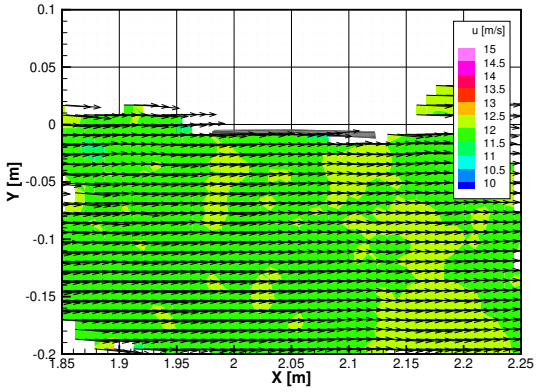

(c) 2D top view at $t/T_{ref} = 0.75$

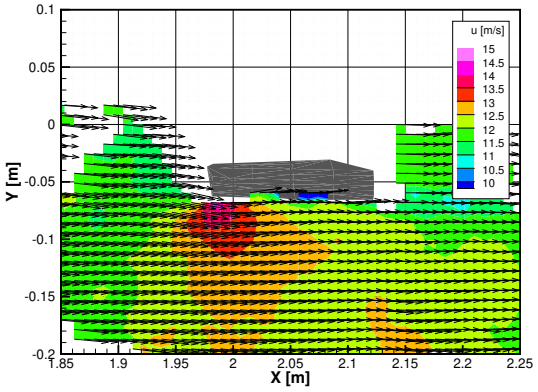

(d) 2D top view at $t/T_{ref} = 1$

Figure 6: Visualization of the FSI phenomenon. Slice cut at $z = 1.147$ m

From the results of the different phases presented, it can be observed that the measured flow field follows coherently the movement of the plate. However, regions of permeation between flow and structure can be

found with a proper 3D inspection of the domain. The cause of those permeation regions can be twofold. One possible reason has to be ascribed to the detection of STB tracks penetrating the structure surface, which is in turn caused by the positional uncertainty of the CVV system. Another more probable cause of the permeation regions stems from the ensemble averaging process. In fact, even if only particles from the correct side of the plate are found, cubic cells spanning across the plate surface and having the centroid beyond it may result in permeating cells when particles fall inside the portion before the plate surface.

A quantitative analysis of the dynamics of the FSI phenomenon is performed. The objective is to assess the relation among the angle of attack induced by the gust field α_{gust}, the angle of attack seen by the plate α_{plate} and the lift generated by the plate. α_{gust} is evaluated as $\alpha_{gust} = \tan^{-1}(-v_{gust}/u_\infty)$, while α_{plate} takes into account the velocity of the plate in the following way: $\alpha_{plate} = \tan^{-1}(-(v_{gust} - v_{plate})/u_\infty)$. Both v_{gust} and u_∞ are evaluated from the data of the slice shown in Figure 6, averaging the values found in the interval $y = [-0.1, 0.1]$ m for $x = 1.925$ m. v_{plate} is the y-velocity of the plate evaluated at the quarter chord point ($x = 2.014$ m) considering the same z location as for the previous calculation. The lift generated by the plate is related to the fluctuation of the streamwise component of the velocity: $u' = u - u_\infty$. u' is evaluated at the point of the flow field closest to the plate point used for the calculation of v_{plate}. A positive value corresponds to the development of a suction side, while a negative value implies a pressure side. The negative sign in the definition of α_{gust} and α_{plate} is purely a convention to have a positive angle of attack corresponding to a positive fluctuation of the velocity. The results of this analysis are shown in Figure 7. It is possible to notice how α_{plate} is slightly shifted in phase with respect to α_{gust} because of the contribution of the plate velocity. As far as u' is concerned, its negative peak coincides in phase with the negative peak of α_{plate}, confirming that $\alpha_{plate} < 0$ induces a pressure over the measured side of the plate. Furthermore, the coincidence of these negative peaks suggests that the lift variation is in phase with α_{plate}, as it is expected given the low reduced frequency of the analyzed case ($k = 0.045$).

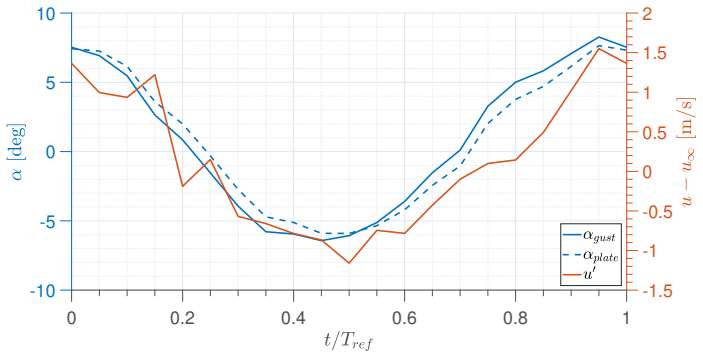

Figure 7: Comparison among α_{gust}, α_{plate} and u'

5 Conclusion

The use of Robotic Volumetric PIV for FSI problems is assessed by means of an experimental investigation conducted at the Open Jet Facility of Delft University of Technology. Phase-averaged structural displacements and flow fields are measured to study the interaction between a periodic gust and a flexible aluminium plate. HFSB are used to seed the flow, whereas small circular markers are applied on the surface of the plate in order to perform the structural measurements. Raw images containing both flow particles and structural markers are processed by means of time-series filters in order to obtain separate sets of images for flow and structure. The PIV structural measurements are validated by means of a Scanning Vibrometer, comparing instantaneous displacements and acceleration. The results show a random error of 0.718 mm and 0.270 mm/s^2 in terms of displacement and acceleration, respectively. The validity of the phase-average approach is assessed considering the average standard deviation of the displacement along the cycle. For the measurement set involving the PIV system with the HFSB seeding, the average standard deviation is equal to 0.717 mm. A visualization of the FSI phenomenon across different phases is presented, together with a quantitative analysis of its dynamics. This demonstrates the ability of the Robotic Volumetric PIV system to identify the phase shift of the angle of attack seen by the plate because of the y-velocity of the plate itself.

References

Agüera N, Cafiero G, Astarita T, and Discetti S (2016) Ensemble 3d PTV for high resolution turbulent statistics. *Measurement Science and Technology* 27:124011

Ballmann J, Dafnis A, Korsch H, Buxel C, Reimerdes HG, Brakhage KH, Olivier H, Braun C, Baars A, and Boucke A (2008) Experimental analysis of high reynolds number structural dynamics in etw. in *46th AIAA Aerospace Sciences Meeting and Exhibit*

Bleischwitz R, de Kat R, and Ganapathisubramani B (2017) On the fluid-structure interaction of flexible membrane wings for MAVs in and out of ground-effect. *Journal of Fluids and Structures* 70:214 – 234

European Commission (2011) Flightpath 2050 Europe's Vision for Aviation. `https://ec.europa.eu/transport/sites/transport/files/modes/air/doc/flightpath2050.pdf`. accessed: 2019-04-03

Jux C, Sciacchitano A, Schneiders JFG, and Scarano F (2018) Robotic volumetric PIV of a full-scale cyclist. *Experiments in Fluids* 59:74

Kalmbach A and Breuer M (2013) Experimental PIV/V3V measurements of vortex-induced fluidstructure interaction in turbulent flowA new benchmark FSI-PfS-2a. *Journal of Fluids and Structures* 42:369 – 387

Lancelot P, Sodja J, and De Breuker R (2017a) Investigation of the unsteady flow over a wing under gust excitation. in *17th International Forum on Aeroelasticity and Structural Dynamics*. IFASD 2017 (Vol. 2017- June). [IFASD-2017-185] International Forum on Aeroelasticity and Structural Dynamics (IFASD)

Lancelot P, Sodja J, Werter N, and De Breuker R (2017b) Design and testing of a low subsonic wind tunnel gust generator. *Advances in Aircraft and Spacecraft Science* 4:125–144

LaVision (2018) *FlowMaster Shake-the-Box (4D PTV)*. LaVision GmbH, Anna-Vandenhoeck-Ring 19, D-37081 Göttingen. Product-Manual. Item-Number(s): 1105075

Lignarolo LEM (2016) *On The Turbulent Mixing in Horizontal Axis Wind Turbine Wakes*. Ph.D. thesis. Delft University of Technology

Marimon Giovannetti L, Banks J, Turnock SR, and Boyd SW (2017) Uncertainty assessment of coupled Digital Image Correlation and Particle Image Velocimetry for fluid-structure interaction wind tunnel experiments. *Journal of Fluids and Structures* 68:125 – 140

Martínez Gallar B, van Oudheusden B, Sciacchitano A, and Karsek M (2018) Large-scale flow visualization of a flapping-wing micro air vehicle. in T Rösgen, editor, *Proceedings 18th International Symposium on Flow Visualization*. ETH Zurich. 18th International Symposium on Flow Visualization (ISFV18); Conference Location: Zurich, Switzerland; Conference Date: June 26-29, 2018

Polytec (2018) Psv-500 scanning vibrometer. `https://www.polytec.com/fileadmin/d/Vibrometrie/OM_DS_PSV-500-1D_E_42445.pdf`. accessed: 2019-03-20

Scarano F, Ghaemi S, Caridi GCA, Bosbach J, Dierksheide U, and Sciacchitano A (2015) On the use of helium-filled soap bubbles for large-scale tomographic piv in wind tunnel experiments. *Experiments in Fluids* 56:42

Schanz D, Gesemann S, and Schröder A (2016) Shake-The-Box: Lagrangian particle tracking at high particle image densities. *Experiments in Fluids* 57:70

Schanz D, Gesemann S, Schröder A, Wieneke B, and Novara M (2012) Non-uniform optical transfer functions in particle imaging: calibration and application to tomographic reconstruction. *Measurement Science and Technology* 24:024009

Schneiders JFG, Scarano F, Jux C, and Sciacchitano A (2018) Coaxial volumetric velocimetry. *Measurement Science and Technology* 29:065201

Sciacchitano A and Scarano F (2014) Elimination of PIV light reflections via a temporal high pass filter. *Measurement Science and Technology* 25:084009

Silva W, Perry B, Florance J, Sanetrik M, Wieseman C, Stevens W, Funk C, Hur J, Christhilf D, and Coulson D (2012) An overview of the semi-span super-sonic transport (s4t) wind-tunnel model program. in *53rd AIAA/ASME/ASCE/AHS/ASC Structures, Structural Dynamics and Materials Conference*

Timpe A, Zhang Z, Hubner J, and Ukeiley L (2013) Passive flow control by membrane wings for aerodynamic benefit. *Experiments in Fluids* 54:1471

TU Delft (2019) Open jet facility. `https://www.tudelft.nl/lr/organisatie/afdelingen/aerodynamics-wind-energy-flight-performance-and-propulsion/facilities/low-speed-wind-tunnels/open-jet-facility/`. accessed: 2019-03-20

Wieneke B (2008) Volume self-calibration for 3d particle image velocimetry. *Experiments in Fluids* 45:549–556

Zhang P, Peterson SD, and M P (2019) Combined particle image velocimetry/digital image correlation for load estimation. *Experimental Thermal and Fluid Science* 100:207 – 221